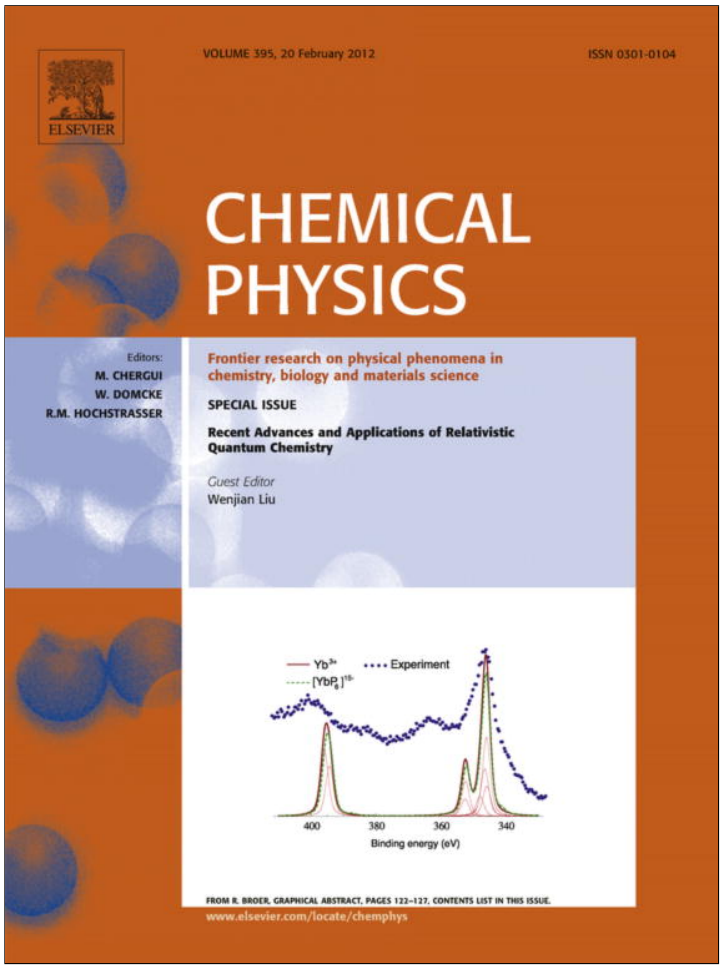

Chemical Physics 395 (2012) 122–127

Contents lists available at ScienceDirect

Chemical Physics

journal homepage: www.elsevier.com/locate/chemphys

Calculation of X-ray photoelectron spectra with the use of the normalized elimination of the small component method

Rob Klooster, Ria Broer *, Michael Filatov

Zernike Institute for Advanced Materials, University of Groningen, Nijenborgh 4, 9747 AG Groningen, Netherlands

ARTICLE INFO

Article history:
Available online 18 May 2011

Keywords:
X-ray photoelectron spectroscopy
Relativistic quantum chemical calculations
Embedded cluster calculations

ABSTRACT

A method for the calculation of X-ray photoelectron spectra (XPS) based on the use of the normalized elimination of the small component (NESC) formalism combined with the restricted active space state interaction (RASSI) approach with atomic mean field integrals (AMFI) is developed. Benchmark calculations carried out for the 4f XPS of U^{5+}show that the NESC/RASSI/AMFI method is capable of reproducing the results of the full 4-component relativistic calculations with excellent accuracy. The NESC/RASSI/AMFI method is applied to study the 4p and 5p XPS of ytterbium phosphide YbP. The results of the calculations suggest an alternative interpretation of the satellite peaks in the 4p XPS of YbP.

1. Introduction

X-ray photoelectron spectroscopy (XPS) provides information on binding energies of the atomic core electrons [1]. The chemical shift of the core electron levels depends on the chemical environment of the ionized atom and on its charge and spin state. However, due to the complicated nature of the interactions of the created hole (empty electron state) with the surrounding electrons, the interpretation of the observed XPS spectra is not straightforward. Accurate first principles calculations can provide important information about these interactions and can assist in the interpretation of the experimental spectra.

The effects of relativity on chemical and physical properties of materials depend strongly on the masses of the constituent atoms [2]. When describing core–hole states, the inclusion of the effects of relativity is mandatory [3–8]. Indeed, relativity strongly modifies the atomic wave function near the nucleus and introduces a substantial energy shift into the electronic energy levels. It seems therefore natural to use the 4-component relativistic formalism based on the Dirac equation [9] to accurately calculate the XPS spectra. The 4-component Dirac–Fock formalism [10–12] is however considerably more complicated than the quantum chemical methods based on the non-relativistic formalism [13]. Even when efficient formulations are implemented [14–18], it can routinely be applied only to the calculation of relatively small systems. For core excitation spectra of larger systems some progress has been made by employing DFT-based initial state methods [19,20]. An alternative is to employ a wave function based quantum chemical method which has computational costs similar to the non-relativistic methods and yet provides accurate account of the relativistic effects.

In the present work, we develop an approach for the calculation of the XPS spectra which is based on the use of the normalized elimination of the small component (NESC) method [21]. Our method of choice is NESC, since it is more accurate than second order Douglas–Kroll, at a lower cost than the infinite order two-component (IOTC) method [22]. When applied in the one-component form [23], this method enables one to treat very large molecular systems. Within this approach, the effect of spin–orbit (SO) coupling is introduced via the restricted active space state interaction (RASSI) method [24] with the use of the atomic mean-field SO integrals (AMFI) [25]. The number of states in the state interaction then limits the size of the systems that can be treated. The intensity of the XPS spectral lines is treated within the sudden approximation [26]. The developed method is benchmarked by the calculation of the 4f XPS of the U^{5+} ion for which the results of accurate 4-component calculations are available. The 4p and 5p XPS spectra of ytterbium phosphide YbP [27] are investigated using the developed method and the role of charge transfer excitations is analyzed.

2. Theory

In this section, the formalism developed in the present work for the calculation of the positions of the XPS spectral lines and of their relative intensities is described. This formalism is based on the NESC method, salient features of which are given below. For a more detailed account, the reader is referred to the original works, Refs. [21,28,29]. The NESC method provides the electronic

* Corresponding author.
E-mail addresses: r.klooster@rug.nl (R. Klooster), r.broer@rug.nl (R. Broer), m.filatov@rug.nl (M. Filatov).

0301-0104/$ - see front matter © 2011 Elsevier B.V. All rights reserved.
doi:10.1016/j.chemphys.2011.05.009

(positive-energy) solutions of the Dirac equation [9] by solving the following eigenvalue equation

$$\widetilde{\mathbf{L}}\mathbf{A} = \widetilde{\mathbf{S}}\mathbf{A}\boldsymbol{\varepsilon} \tag{1}$$

with the relativistic metric given by Eq. (2).

$$\widetilde{\mathbf{S}} = \mathbf{S} + \frac{1}{2c^2}\mathbf{U}^{\dagger}\mathbf{T}\mathbf{U} \tag{2}$$

The eigenvectors $\mathbf{A}$ are normalized on the metric (2) as $\mathbf{A}^{\dagger}\widetilde{\mathbf{S}}\mathbf{A} = \mathbf{I}$, which corresponds to the exact normalization of the large component of the relativistic 4-component wave function.

The NESC Hamiltonian $\widetilde{\mathbf{L}}$ is obtained iteratively by solving the following system of equations [21,29]

$$\widetilde{\mathbf{L}} = \mathbf{T}\mathbf{U} + \mathbf{U}^{\dagger}\mathbf{T} - \mathbf{U}^{\dagger}(\mathbf{T} - \mathbf{W})\mathbf{U} + \mathbf{V} \tag{3}$$

$$\mathbf{U} = \mathbf{T}^{-1}(\mathbf{S}\widetilde{\mathbf{S}}^{-1}\widetilde{\mathbf{L}} - \mathbf{V}) \tag{4}$$

where the elimination of the small component operator $\mathbf{U}$ connects the large $\mathbf{A}$ and the pseudo-large $\mathbf{B}$ components of the modified Dirac wave functions via $\mathbf{B} = \mathbf{U}\mathbf{A}$ [21] In Eqs. (1)–(4), $\mathbf{S}$, $\mathbf{T}$, and $\mathbf{V}$ are the matrices of the overlap, kinetic energy and potential energy operators, and $\mathbf{W}$ is the matrix of the operator $\frac{1}{4c^2}\nabla V(\mathbf{r})\cdot\nabla$ in the basis of the atomic orbitals $\chi_{\mu}(\mathbf{r})$ [21]. The scalar relativistic approximation is used in Eqs. (1)–(4) with the velocity of light c = 137.0359990710(96) [30].

With the use of local atom-centered basis sets which include very tight functions (e.g. the Gaussian type functions with very large exponential factors) the convergence of the iterative solution of the NESC equations may become unstable [29]. It has been therefore suggested to modify Eq. (4) as in Eq. (5)

$$\mathbf{U} = \mathbf{T}^{-1}(\mathbf{S}\mathbf{A}\mathbf{d}\mathbf{A}^{\dagger}\widetilde{\mathbf{L}} - \mathbf{V}) \tag{5}$$

by introducing the diagonal damping matrix $\mathbf{d}$,

$$d_k = \begin{cases} 1, & \varepsilon_k \leqslant 0 \\ (1 + \varepsilon_k/2mc^2), & \varepsilon_k > 0 \end{cases} \tag{6}$$

which damps contributions of the eigenvectors which correspond to the very large positive eigenvalues $\boldsymbol{\varepsilon}$ of (1) of the NESC Hamiltonian.

It is convenient to start the iterative solution of Eqs. (1)–(4) from the solutions of the matrix IORA Eq. (7) [31],

$$\widetilde{\mathbf{L}}^{\mathrm{IORA}}\mathbf{A}^{\mathrm{IORA}} = \widetilde{\mathbf{S}}^{\mathrm{IORA}}\mathbf{A}^{\mathrm{IORA}}\boldsymbol{\varepsilon}^{\mathrm{IORA}} \tag{7}$$

where the Hamiltonian $\widetilde{\mathbf{L}}$ and the metric $\widetilde{\mathbf{S}}$ are obtained using Eq. (8) in Eqs. (3) and (2) [32].

$$\mathbf{U}^{\mathrm{IORA}} = (\mathbf{T} - \mathbf{W})^{-1}\mathbf{T} \tag{8}$$

Eq. (1) provides the exact electronic solutions of the 4-component one-electron problem. To be able to use this solution and the pertinent Hamiltonian operator (3) for the calculation of a many-electron system using a standard non-relativistic quantum chemical code one can employ the one-electron approximation [23] within which the NESC one-electron Hamiltonian renormalized on the non-relativistic metric (9)

$$\mathbf{H}_{1-\mathrm{e}} = \mathbf{S}^{1/2}\widetilde{\mathbf{S}}^{-1/2}\widetilde{\mathbf{L}}\widetilde{\mathbf{S}}^{-1/2}\mathbf{S}^{1/2} \tag{9}$$

is used in connection with the non-relativistic many-electron equations.

The complete active space SCF (CASSCF) method is used for the calculation of the initial state Ψ^I of the target many-electron system. Because with the use of the Hamiltonian (9) only scalar relativistic effects are taken into account, the RASSI approach [24] combined with the AMFI method [25] is used to take the SO effects into account. The wave function Ψ^I of the initial state of the system is then given by a linear combination of the spin-free states as in Eq. (10),

$$\Psi_i^I = \sum_S \sum_{M_S=-S}^{S} \sum_j C_{ij}^{\mathrm{SO}}(S, M_S) \sum_k C_{jk}^{\mathrm{CI}} \Phi_k(S, M_S) \tag{10}$$

where C_{ij}^{SO} are the expansion coefficients of the level Ψ_i^I with a certain value of the total angular momentum J (atomic notation is used throughout the article). This expansion is in terms of spin-free CASSCF wave functions which are characterized by specific values of the total spin S and its projection M_S. The latter wave functions are expanded in terms of the configuration state functions (CSFs) $\Phi_k(S,M_S)$ with the CI coefficients C_{jk}^{CI} obtained in the CASSCF calculation.

The final state Ψ^F of the ionized system is calculated with the use of the restricted active space SCF (RASSCF) formalism whereby the core orbitals from which the ionization occurs are restricted to accommodate one hole and the SO interaction is treated using the RASSI/AMFI approach. Similar to the initial state wave function Ψ^I, the final state wave function Ψ^F is expanded in terms of the spin-free CSFs as in Eq. (11)

$$\Psi_n^F = \sum_{S'} \sum_{M_{S'}=-S'}^{S'} \sum_m C_{nm}^{\mathrm{SO}}(S', M_{S'}) \sum_l C_{ml}^{\mathrm{CI}} \Phi_l(S', M_{S'}) \tag{11}$$

where the summation with respect to the spin S' runs over an extended range of values due to the coupling of the spin of the hole with the spin of the valence shell in the spin-free CSFs $\Phi_l(S', M_{S'})$.

In this work, we are interested in obtaining relative positions of the lines in the XPS spectrum. Therefore, the positions of the spectral lines are determined as the energy differences between the states of the ionized system with different values of the total angular momentum J. The relative intensities of the XPS spectral lines I_{rel} are then calculated using the sudden approximation. The assumption of sudden ionization is valid when the energy of the incident radiation is much greater than the binding energy of the emitted electron. Following Åberg [26], the relative intensity corresponding to the specific final state Ψ^F can be obtained from Eq. (12),

$$I_{rel} \propto \left| \left\langle \hat{a}\Psi^I \mid \Psi^F \right\rangle \right|^2 \tag{12}$$

where the annihilation operator $\hat{a}$ removes an electron from one of the core orbitals without changing the rest of the wave function Ψ^I. Thus, only the CSFs are affected by the annihilation operator in the frozen final state (FFS) $\hat{a}\Psi_I$ and the CI coefficients in the multiconfigurational wave function are left unchanged, Eq. (13). The orbitals used to construct the FFS $\hat{a}\Psi_I$ are identical to the orbitals of the initial state Ψ^I.

$$\hat{a}\Psi_i^I = \sum_S \sum_{M_S=-S}^{S} \sum_j C_{ij}^{\mathrm{SO}}(S, M_S) \sum_k C_{jk}^{\mathrm{CI}} \{\hat{a}\Phi_k(S, M_S)\} \tag{13}$$

Annihilation of one electron in the FFS $\hat{a}\Psi_I$ introduces an extra spin-1/2 in the core orbital which can be coupled in two different ways with the open shell valence electrons. Given that a CSF in the expansion of the initial state Ψ^I, Eq. (10) has total spin S, the CSFs with the total spin $S + 1/2$ and $S - 1/2$ emerge in the FFS $\hat{a}\Psi_I$. The contributions of the new CSFs into the FFS wave function can be derived using the "genealogical" construction [33], that is by successive coupling of the individual spins in the open shell orbitals with the spin in the ionized orbital. When deriving the FFS expansion in terms of CSFs, Eq. (14), both directions of the extra spin in the ionized orbitals, α and β, were taken with equal weights.

$$\hat{a}\Psi_i^I = \sum_S \sum_{M_S=-S}^{S} \sum_j C_{ij}^{SO}(S,M_S) \sum_k C_{jk}^{CI} \times$$

$$\left\{ \sqrt{\frac{S+M_S+1}{4S+2}} \Phi_k(S+1/2, M_S+1/2) \right. \quad (14a)$$

$$+\sqrt{\frac{S-M_S+1}{4S+2}} \Phi_k(S+1/2, M_S-1/2) \quad (14b)$$

$$-\sqrt{\frac{S-M_S}{4S+2}} \Phi_k(S-1/2, M_S+1/2) \quad (14c)$$

$$\left. +\sqrt{\frac{S+M_S}{4S+2}} \Phi_k(S-1/2, M_S-1/2) \right\} \quad (14d)$$

Eq. (14) yields the expansion of the FFS $\hat{a}\Psi_I$ in terms of the CSFs with the same total spin S and projection of the spin M_S as appear in the expansion of the final state Ψ^F, Eq. (11). Therefore the relative intensities of the XPS spectral lines can be calculated from the overlap integrals between the CSFs with the same spin symmetry and the CI and SO expansion coefficients in Eq. (14) and (11).

3. Details of calculations

The described formalism was implemented into a development version of the MOLCAS7 suite of programs [34]. For the calculations on uranium, we employ Dyall's double-zeta basis set [35] which has been uncontracted and augmented with polarizing and correlating functions. This basis set is of comparable size and quality as the basis set used in four-component calculations by Bagus [6]. The calculations on YbP employ the ANO-RCC double-zeta polarized basis set on ytterbium [36] and on phosphorous [37].

When calculating the XPS spectrum of U^{5+}, a CASSCF calculation with 1 electron distributed over 7 active orbitals (denoted as (1,7) CASSCF) was carried out for the initial state in the configuration (Rn)$5f^1$. The final state of the ionized atom U^{6+}, in (Rn)$4f^{-1}5f^1$ configuration, was calculated using a (14,14) RASSCF formalism whereby the 5f-orbitals occupied with one electron were put in RAS2 and 4f-orbitals occupied with 13 electrons were put in RAS1. RAS1 in these calculation was restricted to accommodate maximum one hole. The core orbitals were kept frozen in the RASSCF calculations.

Ytterbium phosphide YbP has the rock salt crystal structure with space group $Fm\bar{3}m$ and a lattice constant of 5.5461 ± 0.0005 Å at 295 K [38]. The calculations were carried out in the embedded cluster approximation [39] where a YbP_6^{15-} cluster (Y–B bond length 2.773 Å) was embedded in the field of an array of ab initio model potentials (AIMP) [40] and point charges. The formal valences of the atoms in YbP were taken as the magnitudes of the point charges modeling the crystal lattice. The array of point charges of the length of five lattice constants in each crystallographic direction was constructed whereby the surface point charges were renormalized using Evjen's scheme [41]. To make the description of the immediate coordination sphere of the cluster more realistic, all the atoms within the radius of 7.5 Å from the central atom were described by the respective AIMPs. The potentials were obtained from fitting the potential of a single atomic ion, Yb or P, embedded in the array of atomic ions described by the same model potential. When modeling the charge distribution of the atomic ions, 15 spherical symmetric Gaussian-type functions were used on ytterbium and 11 functions on phosphorous. For comparison, the calculations were also carried out for a free Yb^{3+} cation.

The initial state of the Yb^{3+} cation was calculated using the (13,7) CASSCF wave function whereby the 4f-orbitals of Yb occupied with 13 electrons are included into the active space. For the final states of the ionized Yb^{4+}, the (18,10) RASSCF calculations were carried out in which 13 electrons in 4f-orbitals are taken into the RAS2 and 5 electrons in 5p-orbitals are taken into the RAS3, for the case of the 5p-hole (5 electrons in 4p-orbitals, for the case of the 4p-hole). For YbP_6^{15-} cluster, the RAS2 active space included 13 electrons in the 4f-orbitals of Yb and 24 electrons in the odd (*ungerade*) symmetry adapted linear combinations of the 3s and 3p-orbitals of P. For the ionized YbP_6^{14-} cluster, the so-obtained (37,19) active space in RAS2 was augmented by the (5,3) active space in RAS3. The latter was set up similarly to the Yb^{4+}cation. The RAS3 space was restricted to accommodate at most five electrons. In all final states, the open shell core orbitals were kept frozen during the RASSCF calculations.

For comparison, the free ion calculations were repeated within a four-component formalism, using the program DIRAC10 [42]. These calculations employ Dyall's double-zeta basis set [35,43], which has been uncontracted and augmented with polarizing and correlating functions and include the Breit term in the two-electron interaction. Only binding energies could be calculated, not the intensities.

4. Results and discussion

4.1. Uranium 4f XPS

As a test case, we calculate the 4f XPS spectrum of the U^{5+}ion. The initial state has the single valence electron distributed over all 5f orbitals, which gives a ^2F multiplet. When we include SO coupling, this multiplet splits into a $^2F_{5/2}$ ground state and a $^2F_{7/2}$ excited state separated by 1.0 eV (0.90 eV from 4C calculation). This splitting is large enough to assume that the system is completely in the ground state at room temperature.

The singlet state with lowest energy in the calculation of the final state corresponds to the ground state of closed shell U^{6+} (^1S). The orbitals are optimized to minimize the average energy of all singlet states *except* this closed shell state. In the triplet case, all states are included in the orbital optimization. The 4f orbitals are kept frozen in both singlet and triplet calculations to prevent collapse to 5p-ionized states. The resulting Russel–Saunders terms are ^{1,3}S, ^{1,3}P, ^{1,3}D, ^{1,3}F, ^{1,3}G, ^{1,3}H and ^{1,3}I. Afterwards, the SO-split states are calculated as described in Section 2, yielding states of $J = 0, \ldots, 7$.

The relative ionization intensities are calculated from the sudden approximation as described above. The spin-free frozen final states are linear combinations of singlet and triplet states, with relative weights 1/4 and 3/4 respectively. If the SO coupling were taken into account from the beginning, the initial state would only have the $5f_{5/2}$ component occupied with a single electron. This would result in $4f_{7/2}^{-1}5f_{5/2}^1$ and $4f_{5/2}^{-1}5f_{5/2}^1$ as the only XPS allowed final state configurations. One can have levels with $J = 1, 2, 3, 4, 5, 6$ in the first configuration, and with $J = 0, 1, 2, 3, 4, 5$ in the second. In our calculation, also the configurations $4f_{7/2}^{-1}5f_{7/2}^1$ and $4f_{5/2}^{-1}5f_{7/2}^1$ are included, because in the spin-free calculation all 5f orbitals are equivalent. These configurations do not carry any intensity, but can still contribute to the XPS allowed final states through configuration mixing, as long as the total J is the same. This leads to "intensity stealing", i.e. the states which have predominant $5f_{5/2}^1$ character will lose some intensity by mixing in $5f_{7/2}^1$ configurations, and the states which have predominant $5f_{7/2}^1$ character will gain some intensity by mixing in $5f_{5/2}^1$ configurations. The $J = 7$ level, which arises from the coupling of the $4f_{7/2}$ hole to the $5f_{7/2}$ electron (in LS terms, from ^{3}I), is the only XPS forbidden level and hence has an intensity equal to zero. Indeed, the contributions of the spin-free intensities to this SO level cancel.

For the final states, two types of calculations have been performed. In the first type, the orbitals of the final state were kept

identical to the IS and only the CI coefficients were optimized. The results for the most important peaks are summarized in Table 1. In the second calculation, all orbitals, except the 4f orbitals from which the ionization takes place, were allowed to relax (Table 2). This allows us to estimate the effects due to orbital relaxation in the final state. It also allows us to make a detailed comparison to the results of the full four-component (4C) DCI and DF-SCF methods by Bagus and Ilton [6].

The intensity of a level is summed over all M_J states, the maximum intensity of a given level is equal to its multiplicity ($2J + 1$). The intensities lost to satellites due to configuration mixing and orbital relaxation are also given in the tables, in percentages.

Both types of calculations show two dominant structures originating from the ionization from either the $4f_{7/2}$ (0–3 eV) or the $4f_{5/2}$ orbital (10–30 eV). There is an excellent agreement in relative energies between the NESC/RASSI/AMFI results and the 4C results within the $4f^{-1}_{7/2}$ and $4f^{-1}_{5/2}$ structures, but the splitting between the two structures is 5–8% smaller in our results. The relative intensities of the shown multiplets is smaller in our results compared to the 4C results, which suggests more intensity "stealing" in our calculations.

Orbital relaxation has an effect on both the relative binding energies as well as the relative intensities. The splitting within both the $4f_{5/2}$ and the $4f_{7/2}$ structures increases. This is caused by the reduced shielding of the nuclear charge in the final state, which makes the 5f orbitals more compact, the 4f–5f Coulomb interactions larger, leading to larger splittings. There is also an overall decrease in intensity of the peaks, since orbital relaxation allows intensity "stealing" by satellites.

The decrease in the energy separation of the two structures as compared to the 4C results may be partly attributed to the neglect of the Breit interaction in the 4C calculations. This interaction is responsible for the spin-other-orbit interaction in AMFI and is therefore partly included in our calculations. However, including the full Breit interaction in the 4C calculation only lowers the SO splitting by less than 0.4 eV. The remainder can be attributed to the fact that the difference of the $f_{5/2}$ and $f_{7/2}$ orbitals is not sufficiently accurately reproduced in RASSI/AMFI calculations. In our results, the 4f orbitals have approximately the radial dependence of the average of the $4f_{5/2}$ and $4f_{7/2}$ orbitals. These orbitals are more similar to the $4f_{7/2}$ orbitals, because they contribute more to the average. This means that the effect of orbital relaxation is greater for the $4f_{5/2}$ orbitals, which results in a larger SO splitting. The difference in intensities can be explained by the similar radial dependence of the 5f orbitals, which makes the mixing of the $5f^1_{5/2}$ and $5f^1_{7/2}$ configurations more efficient in our calculations. Therefore more intensity is lost to satellites of $5f_{7/2}$ character, compared to the full 4C calculations.

Table 1
Relative excitation energies and relative intensities for the main peaks of the 4f XPS of U^{5+} using NESC/RASSI/AMFI compared to the full 4 component DCI results of Bagus et al. [6]. The orbitals of the final state were kept identical to the initial state. For the $4f_{5/2}$ peaks, also the energy relative to the first $4f_{5/2}$ peak is given. The relative intensities are summed over all M_J states. The percentage of intensity lost to satellites is also given.

J	$E_{rel}/\Delta E_{rel}$(eV)	$E^{4C}_{rel}/\Delta E^{4C}_{rel}$ (eV)	I_{rel}	lost I(%)	I^{4C}_{rel}	lost I(%)
$4f^{-1}_{7/2}$						
1	0	0	2.66	11.3	2.78	7.4
2	0.92	0.93	4.58	8.4	4.70	6.0
6	0.96	0.94	12.79	1.6	12.85	1.2
3	1.50	1.52	6.44	8.0	6.68	4.5
4	1.91	1.91	8.79	2.4	8.87	1.4
5	1.95	1.96	10.99	0.1	10.99	0.1
$4f^{-1}_{5/2}$						
1	10.93/0	11.83/0	2.44	18.7	2.70	10.0
5	11.37/0.44	12.24/0.40	10.79	1.9	10.84	1.4
3	12.21/1.29	13.08/1.25	6.87	1.9	6.94	0.9
2	12.30/1.37	13.18/1.35	4.58	8.4	4.91	1.8
4	12.55/1.62	13.42/1.58	9.00	0.0	9.00	0.0
0	25.28/14.35	26.13/14.30	0.68	32.3	0.69	31.0

Table 2
Relative excitation energies and relative intensities for the main peaks of the 4f XPS of U^{5+} using NESC/RASSI/AMFI compared to the full 4 component DF-SCF results of Bagus et al. [6]. The difference with respect to the results in Table 1 is that the orbitals of the final state were allowed to relax in the presence of the frozen core hole.

J	$E_{rel}/\Delta E_{rel}$(eV)	$E^{4C}_{rel}/\Delta E^{4C}_{rel}$ (eV)	I_{rel}	lost I(%)	I^{4C}_{rel}	lost I(%)
$4f^{-1}_{7/2}$						
1	0	0	2.51	16.3	2.67	11.1
2	1.12	1.08	4.32	13.6	4.58	8.3
6	1.18	1.11	12.02	7.54	12.80	1.5
3	1.81	1.75	6.10	12.8	6.44	8.0
4	2.28	2.22	8.27	8.1	8.79	2.3
5	2.33	2.26	10.30	6.4	10.99	0.1
$4f^{-1}_{5/2}$						
1	11.07/0	11.63/0	2.35	21.7	2.48	17.4
5	11.56/0.49	12.13/0.50	10.13	7.9	10.80	1.9
3	12.56/1.49	13.09/1.46	6.47	7.6	6.88	1.8
2	12.71/1.64	13.21/1.58	4.49	10.2	4.64	7.2
4	12.96/1.89	13.48/1.85	8.43	6.3	8.99	0.0
0	29.25/18.19	28.38/16.75	0.59	41.0	0.66	34.2

4.2. Yb 4p/5p XPS

YbP has a NaCl-type structure with formal charges of $Yb^{3+}$and P^{3-}. We have calculated the 4p and 5p XPS of Yb in YbP. As model systems we used a single ion $Yb^{3+}$and a cluster $[YbP_6]^{15-}$, embedded in ab initio model potentials and point charges. The results are compared to the experimental spectrum of Saitoh et al. [27].

The initial state valence configuration of $Yb^{3+}$is $4f^{13}$. This gives rise to a $^2F_{7/2}$ ground state and a $^2F_{5/2}$ excited state, split by 1.3 eV. This splitting is large enough to ensure that the system is completely in the ground state at room temperature. In the cluster the initial state splits further due to the octahedral environment by about 0.05 eV and the system can be described by a Boltzmann distribution over the lowest states.

Ionization takes place from the 4p or 5p shell with $j = 1/2$ or $3/2$, which couples to the initial $J = 7/2$ to yield XPS allowed states of $J = 3$, 4 and $J = 2$, 3, 4, 5, respectively. In the cluster, the increased charge on Yb after ionization stabilizes charge transfer (CT) configurations in which electrons of the surrounding P 3p orbitals are donated to the central Yb 4f orbital. These Yb ($4/5p^54f^{14}$) $\underline{L}$ CT configurations can mix with the Yb ($4/5p^54f^{13}$) non-CT configurations and this may give rise to extra features in the spectrum. All orbitals, except the core orbital from which the ionization takes place, are optimized to minimize the average energy of all (non-CT and CT) states. The obtained peaks are broadened by a gaussian and lorentzian distribution to model the lifetime and Doppler broadenings. Moreover the spectrum is shifted rigidly so that the most intense peak aligns with the experimental peak.

The calculated 5p XPS spectrum is shown in Fig. 1. Comparison with the experimental spectrum shows that the calculated SO splitting between the $5p_{1/2}$ and $5p_{3/2}$ peaks is $\sim$ 0.4 eV smaller in $Yb^{3+}$and $\sim$1.2 eV smaller in the cluster. The SO splitting in the cluster is smaller because the core–hole is slightly hybridized with the valence P orbitals. Another difference with the free ion is the occurrence of CT states in the cluster. These states contribute to the intensity, but this effect is hidden under the main peaks. The computed relative intensities are very close to the 2:1 statistical weight ratio of $5p_{1/2}$ and $5p_{3/2}$. In the experimental spectrum the $5p_{1/2}$

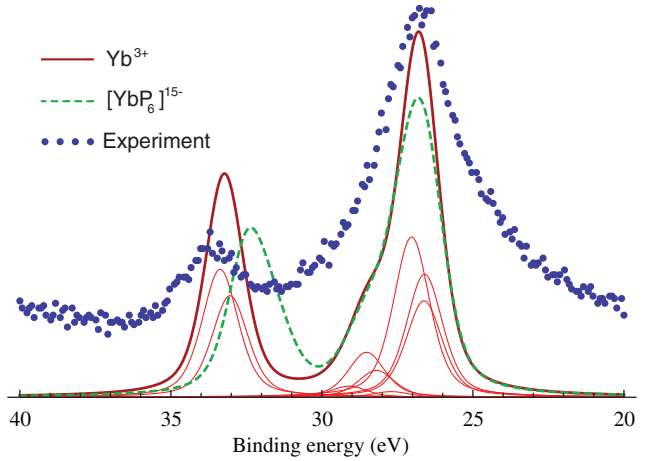

Fig. 1. The calculated 5p XPS spectra of Yb^{3+} and $[YbP_6]^{15-}$. Contributions of the individual *J*-states are shown for the free ion calculation. All individual peaks have been broadened by a 1 eV FWHM gaussian and a 0.7 eV FWHM lorentzian. The calculated spectra have been rigidly shifted by −34.3 eV for Yb^{3+} and + 1.4 eV for $[YbP_6]^{15-}$. The experimental spectrum has been taken from Ref. [27].

peak is less intense than expected from the intensity of the $5p_{3/2}$ peak. This difference can be attributed to the neglect of higher lying configurations in the CI expansion. These can mix more with the $5p^{-1}_{1/2}$ states, and therefore "steal" more intensity from this peak.

The difference in SO splitting in the 5p shell can be explained by the difference in radial dependence of the $5p_{1/2}$ and $5p_{3/2}$ orbitals, which is not accurately treated in the RASSI/AMFI method. Indeed, when we calculate the energies of the 5p ionized states in the Yb^{3+}ion using a 4C scheme, the 5p SO splitting increases by about 0.9 eV. In the free ion calculation, the error due to the incorrect radial behavior of the 5p orbitals is mostly compensated by the error due to the neglect of the crystal environment.

The calculated 4p XPS spectrum is shown in Fig. 2. The splitting between the $4p_{1/2}$ and the $4p_{3/2}$ structures is ∼6 eV smaller than the experimental splitting, while the splitting between the two peaks of the $4p_{3/2}$ structure is ∼10 eV smaller. In the cluster calculation the splittings are similar to the free ion calculation, but two

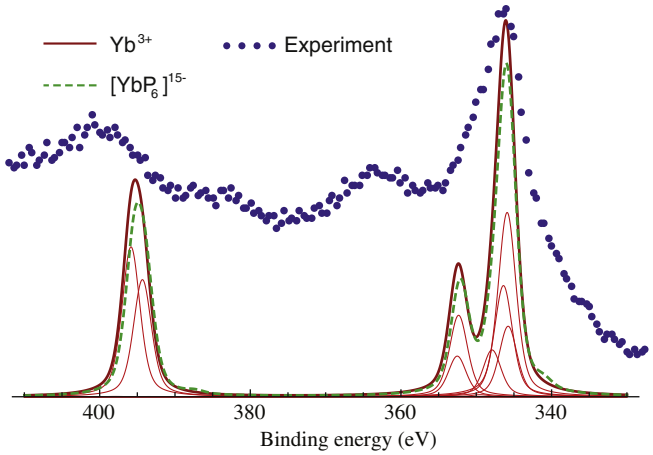

Fig. 2. The calculated 4p XPS spectra of Yb^{3+} and $[YbP_6]^{15-}$. Contributions of the various *J*-states are shown for the free ion calculation. All individual peaks have been broadened by a 2 eV FWHM gaussian and a 1.4 eV FWHM lorentzian. The calculated spectra have been rigidly shifted by −41.4 eV for Yb^{3+} and −8.6 eV for $[YbP_6]^{15-}$. The experimental spectrum has been taken from Ref. [27].

extra peaks at 341 eV and 387 eV emerge. Mulliken population analysis shows that these peaks originate from transitions to CT states with an Yb $4f^{14}$ occupation, as opposed to the non-CT states of the main peaks with an Yb $4f^{13}$ occupation. The binding energies of the CT states are thus smaller than the non-CT states. The core ionization introduces extra positive charge on the Yb atom, which stabilizes those configurations in which an electron is transfered from a P 3p orbital to Yb 4f more than non-CT configurations. In the initial state, the CT states are only ∼5 eV higher in energy than the ground state, so upon ionization these states drop below the non-CT states. The calculated intensities of the CT states are very small, but it is expected that if the relaxation of a greater part of the crystal were taken into account, these contributions would become more important.

The calculated binding energies of the Yb^{3+} ion have been compared to a full 4C calculation, which shows that the SO splitting of the core orbitals has been underestimated by about 3.9 eV in our NESC/RASSI/AMFI calculation, for the same reasons as in the 5p XPS. The splittings within the two structures, in particular within the $4p_{3/2}$ structure, were reproduced accurately. The discrepancy between the experiment and our calculations may be explained by electron correlation effects, in particular the neglect of so-called frustrated Auger configurations which are missing in the present calculations. It has been shown [4,7] that these configurations, in which there is a simultaneous excitation of a valence electron to a higher lying orbital and a de-excitation of an electron into the core–hole, may have a large effect on the relative binding energies.

In the experimental spectrum, the peak at 386 eV and the shoulder around 338 eV were attributed to surface Yb^{2+}contributions [27]. From our calculations it can be seen that these may instead originate from CT states.

5. Conclusions

The necessity to model XPS spectra of large clusters requires the use of computational methods that are capable of providing accurate results at a low or moderate cost. The method developed in the present work is based on the exact transformation of the full 4-component relativistic formalism to a two-component form using the NESC approach developed previously [21,29]. The spin-scalar NESC method is combined with the RASSI/AMFI approach [24,25] to describe the effect of spin–orbit coupling in the initial and in the final states of systems undergoing ionization of the core electrons. The relative intensities of the spectral lines in the XPS spectra are then calculated using the sudden approximation [26].

The developed approach was benchmarked by the calculation of the 4f XPS spectra of U^{5+}cation for which the results of full 4-component relativistic calculations are available [5,6]. The multiplet splittings and the relative intensities of the 4f XPS spectra of U^{5+}calculated using the NESC/RASSI/AMFI approach are in a generally excellent agreement with the results of 4-component calculations. A slight underestimation (*ca.* 10%) of the magnitude of the splitting between the $4f_{5/2}$ and $4f_{7/2}$ states can be attributed to an insufficient account of spin–orbit interaction via the RASSI/AMFI approach which was designed to treat the SO splittings in the valence shells of compounds of heavy elements [24].

The study of the 5p and 4p XPS spectra of YbP has revealed that the crystalline environment has greater influence on the ionization of the sub-valence (5p) shell. It was also found that ionization of the 4p shell is sensitive to the effect of ligand–metal charge transfer. The latter may be responsible for the occurrence of satellite peaks in the 4p XPS spectrum at 386 eV and at 338 eV which were previously attributed to the contribution of surface Yb^{2+}cations [27].

Acknowledgment

Prof. P.S. Bagus is thanked for many helpful discussions and for making the results of his calculations available to us. The authors would also like to thank Prof. S. Suga and Dr. Y. Saitoh for providing the experimental spectra.

References

[1] C. Nordling, E. Sokolowski, K. Siegbahn, Phys. Rev. 105 (1957) 1676.
[2] M. Barysz, Y. Ishikawa (Eds.), Relativistic Methods for Chemists, Challenges and Advances in Computational Chemistry and Physics, Vol. 10, Springer, 2010.
[3] P.S. Bagus, R. Broer, W.A. de Jong, W.C. Nieuwpoort, F. Parmigiani, L. Sangaletti, Phys. Rev. Lett. 84 (2000) 259.
[4] P.S. Bagus, R. Broer, E.S. Ilton, Chem. Phys. Lett. 394 (2004) 150.
[5] E.S. Ilton, P.S. Bagus, Phys. Rev. B 71 (2005) 195121+.
[6] P.S. Bagus, E.S. Ilton, Theor. Chem. Acc. 118 (2007) 495.
[7] P.S. Bagus, R. Broer, E.S. Ilton, J. El. Spectr. Rel. Phen. 165 (2008) 46.
[8] R. Broer, Relativistic Methods for Chemists, in: M. Barysz, Y. Ishikawa (Eds.), Challenges and Advances in Computational Chemistry and Physics, vol. 10, Springer, 2010, p. 351.
[9] P.A.M. Dirac, Proc. Roy. Soc. (London) A117 (1928) 610.
[10] B. Swirles, Proc. Roy. Soc. (London) A152 (1935) 625.
[11] P. Hafner, J. Phys. B: Atom. Molec. Phys. 13 (1980) 3297.
[12] L. Visscher, O. Visser, P.J.C. Aerts, H. Merenga, W.C. Nieuwpoort, Comp. Phys. Comm. 81 (1994) 120.
[13] W. Liu, Mol. Phys. 108 (2010) 1679.
[14] T. Fleig, J. Olsen, C.M. Marian, J. Chem. Phys. 114 (2001) 4775.
[15] T. Fleig, J. Olsen, L. Visscher, J. Chem. Phys. 119 (2003) 2963.
[16] T. Fleig, H. Jensen, J. Olsen, L. Visscher, J. Chem. Phys. 124 (2006) 104106.
[17] L. Visscher, J. Comp. Chem. 23 (2002) 759.
[18] M. Pernpointer, L. Visscher, W.A. de Jong, R. Broer, J. Comp. Chem. 21 (2000) 1176.
[19] U. Ekström, P. Norman, Phys. Rev. A 74 (2006) 042722.
[20] S. Villaume, T. Saue, P. Norman, J. Chem. Phys. 133 (2010) 064105.
[21] K.G. Dyall, J. Chem. Phys. 106 (1997) 9618.
[22] M. Barysz, A. Sadlej, J. Chem. Phys. 116 (2002) 2696.
[23] K.G. Dyall, J. Comp. Chem. 23 (2002) 786.
[24] P.-Å. Malmqvist, B.O. Roos, B. Schimmelpfennig, Chem. Phys. Lett. 357 (2002) 230.
[25] B. Schimmelpfennig, L. Maron, U. Wahlgren, C. Teichteil, H. Fagerli, O. Gropen, Chem. Phys. Lett. 286 (1998) 267.
[26] T. Åberg, Phys. Rev. 156 (1967) 35.
[27] Y. Saitoh, S. Suga, H. Matsubara, Y. Tsukikawa, Y. Mori, A. Oyamada, A. Ochiai, T. Suzuki, T. Kasuya, J. Phys. Soc. Jpn 60 (1991) 4005.
[28] M. Filatov, J. Chem. Phys. 125 (2006) 107101.
[29] M. Filatov, K.G. Dyall, Theor. Chem. Acc. 117 (2007) 333.
[30] G. Gabrielse, D. Hanneke, T. Kinoshita, M. Nio, B. Odom, Phys. Rev. Lett. 97 (2006) 030802.
[31] K.G. Dyall, E. van Lenthe, J. Chem. Phys. 111 (1999) 1366.
[32] M. Filatov, D. Cremer, J. Chem. Phys. 122 (2005) 064104.
[33] R. Paunch, Spin Eigen Functions, Plenum Press, New York, 1979.
[34] F. Aquilante, L. De Vico, N. Ferré, G. Ghigo, P.-Å. Malmqvist, P. Neogrády, T.B. Pedersen, M. Pitonak, M. Reiher, B.O. Roos, L. Serrano-Andrés, M. Urban, V. Veryazov, R. Lindh, J. Comp. Chem. 31 (2010) 224.
[35] K.G. Dyall, Theor. Chem. Acc. 117 (2007) 491. Available from the Dirac web site, <http://dirac.chem.vu.nl>.
[36] B.O. Roos, R. Lindh, P.-Å. Malmqvist, V. Veryazov, P.-O. Widmark, J. Phys. Chem. A 112 (2008) 11431.
[37] B.O. Roos, R. Lindh, P.-Å. Malmqvist, V. Veryazov, P.-O. Widmark, J. Phys. Chem. A 108 (2005) 2851.
[38] A. Dönni, P. Fischer, A. Furrer, P. Bonville, F. Hulliger, H.R. Ott, Z. Phys. B – Cond. Matter 81 (1990) 83.
[39] A. Shukla, M. Dolg, H. Stoll, P. Fulde, Chem. Phys. Lett. 262 (1996) 213.
[40] L. Seijo, Z. Barandiarán, in: J. Leszczynski (Ed.), Computational Chemistry: Reviews of Current Trends, vol. 4, World Scientific, Singapore, 1999, p. 55.
[41] H.M. Evjen, Phys. Rev. 39 (1932) 675.
[42] DIRAC, a relativistic ab initio electronic structure program, Release DIRAC10, (2010). Written by T. Saue, L. Visscher and H.J. Aa. Jensen, with contributions from R. Bast, K.G. Dyall, U. Ekström, E. Eliav, T. Enevoldsen, T. Fleig, A.S.P. Gomes, J. Henriksson, M. Iliaš, Ch. R. Jacob, S. Knecht, H.S. Nataraj, P. Norman, J. Olsen, M. Pernpointner, K. Ruud, B. Schimmelpfennig, J. Sikkema, A. Thorvaldsen, J. Thyssen, S. Villaume, and S. Yamamoto (see <http://dirac.chem.vu.nl>).
[43] A.S.P. Gomes, L. Visscher, K.G. Dyall, Theor. Chem. Acc. 127 (2010) 369. Available from the Dirac web site, <http://dirac.chem.vu.nl>.